Chinese Chemical Letters 35 (2024) 108739

Contents lists available at ScienceDirect

Chinese Chemical Letters

journal homepage: www.elsevier.com/locate/cclet

Tuning SMSI to stabilize metallic Pd species: A case study on Pd/TiO_2 for HCHO oxidation

Chunying Wang[a,b], Xiaofeng Liu[a], Jingyi Wang[a,b], Yaobin Li[a,b,*], Shaohua Xie[c], Fudong Liu[c], Changbin Zhang[d], Yuming Zheng[a], Wenpo Shan[a,b,*], Hong He[a,b,d]

[a] *Center for Excellence in Regional Atmospheric Environment, Key Laboratory of Urban Pollutant Conversion, Institute of Urban Environment, Chinese Academy of Sciences, Xiamen 361021, China*
[b] *Zhejiang Key Laboratory of Urban Environmental Processes and Pollution Control, Ningbo Urban Environment Observation and Research Station, Chinese Academy of Sciences, Ningbo 315800, China*
[c] *Department of Civil, Environmental, and Construction Engineering (CECE), Catalysis Cluster for Renewable Energy and Chemical Transformations (REACT), Nano Science Technology Center (NSTC), University of Central Florida, Orlando, FL 32816, USA*
[d] *State Key Joint Laboratory of Environment Simulation and Pollution Control, Research Center for Eco-environmental Sciences, Chinese Academy of Sciences, Beijing 100085, China*

ARTICLE INFO

Article history:
Received 8 January 2023
Revised 12 June 2023
Accepted 25 June 2023
Available online 28 June 2023

Keywords:
Pd/TiO_2
Surface defects
SMSI
Formaldehyde
Stability of Pd species

ABSTRACT

Pretreatment of the carrier for supported catalysts can effectively improve the strong metal-support interaction (SMSI) and increase the dispersion of precious metals, which are critical to many important catalytic reactions. In this work, we tuned SMSI on Pd/TiO_2 catalysts through inducing surface defects of TiO_2 by pretreated with different atmospheres (H_2/N_2, N_2, O_2/N_2) at the high temperature (800 °C). Multiple characterization results illustrated that surface defects anchored Pd species and thus enhanced their dispersion. During reduction, Ti^{3+} species formed and transferred onto the metallic Pd species and then induced SMSI, which effectively stabilize Pd species in the metallic state. The stronger MSI, the more stability of Pd species. As a case, Pd/TiO_2–$800H_2$, with strongest MSI, displayed the best HCHO oxidation performance at low temperature (10 °C).

© 2023 Published by Elsevier B.V. on behalf of Chinese Chemical Society and Institute of Materia Medica, Chinese Academy of Medical Sciences.

In noble metal catalyst systems, the strong metal support interaction (SMSI), firstly proposed by Tauster *et al.* [1], is extremely important for catalytic reactions [2–5]. The phenomenon is caused by the migration of partially oxidized carrier material onto the surface of metal nanoparticles under reduction treatment because of the increase in the surface energy of the metal particles [2,6]. In this process the formation of suboxide species is necessary [2]. Typically, SMSI can trigger a series of changes on catalysts, including encapsulation of metal NP_S by an oxide layer at high temperature [7,8], enhanced bonding between the supported metal and the oxide carrier [9] and accelerated electron transfer between the supported metal and the oxide carrier [10]. It can be concluded that with the construction of SMSI, a new and highly active interface may be generated and the dispersion of the loaded metal can be improved to some extent. According to current reports, the SMSI can be constructed and regulated by changing the type of carrier oxide [11,12], modification by doping [13] or creating surface defects on the carrier oxide [14], *etc.* Among these strategies, the creation of carrier defects is a common and effective method [15–17].

Formaldehyde (HCHO) is regarded as a major indoor pollutant emitted from buildings, furnishing materials and consumer products [18,19]. It poses a potential health risk to occupants even at very low concentration levels [20]. Thus, it is necessary to develop suitable techniques to solve indoor air HCHO pollution. Researchers have investigated plant purification [21,22], adsorption [23], photocatalysis [24–26], plasma [27,28], catalytic oxidation [29,30] and other technologies. Among these, catalytic oxidation is one of the technologies with the most potential, especially when using supported noble metal catalysts, which can completely oxidize HCHO into CO_2 and H_2O at room temperature. However, the high cost of supported noble metal catalysts limits their wide application. Therefore, further improving the performance of catalysts and reducing cost has been the focus of research in recent years.

Titanium dioxide (TiO_2), as a reducible oxide, is an excellent support for noble metal catalysts, on which SMSI can be induced. Previous studies have shown that high temperature reduction treatment of TiO_2 is a good strategy to create defect sites and

* Corresponding authors at: Center for Excellence in Regional Atmospheric Environment, Key Laboratory of Urban Pollutant Conversion, Institute of Urban Environment, Chinese Academy of Sciences, Xiamen 361021, China.
E-mail addresses: ybli@iue.ac.cn (Y. Li), wpshan@iue.ac.cn (W. Shan).

https://doi.org/10.1016/j.cclet.2023.108739
1001-8417/© 2023 Published by Elsevier B.V. on behalf of Chinese Chemical Society and Institute of Materia Medica, Chinese Academy of Medical Sciences.

Table 1
Specific surface area (BET), Pd dispersion (D_{TEM}), mean particles size (d_{Pd}) and TOFs of Pd/TiO_2, Pd/TiO_2–$800H_2$, Pd/TiO_2–$800N_2$ and Pd/TiO_2–800Air samples.

Samples	S_{BET} (m^2/g)	D_{TEM}[a] (%)	d_{Pd} (nm)	TOF × 10^{-2} (s^{-1})
Pd/TiO_2	33.0	–	–	–
Pd/TiO_2–$800H_2$	8.2	74.80%	1.5	2.68
Pd/TiO_2–$800N_2$	12.5	33.02%	3.3	1.69
Pd/TiO_2–800Air	13.8	31.18%	3.4	1.12

[a] Pd dispersion based on TEM data; the detailed calculation is shown in Supporting information.

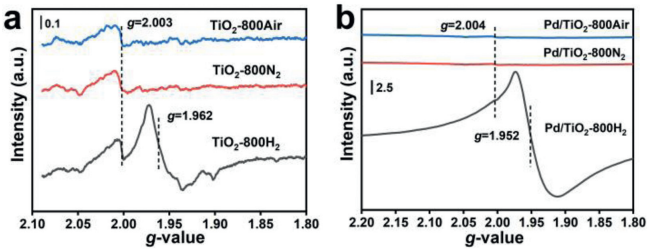

Fig. 1. The ESR spectra of (a) TiO_2–$800H_2$, TiO_2–$800N_2$, TiO_2–800Air carries and (b) Pd/TiO_2–$800H_2$, Pd/TiO_2–$800N_2$, Pd/TiO_2–800Air catalysts.

induce SMSI [31,32]. Meanwhile, the catalytic oxidation capability for HCHO at room temperature was found to mainly result from surface hydroxyl groups and chemisorbed oxygen species [32,33], and is also related to surface defects (*e.g.*, oxygen vacancies) and active metal sites (*e.g.*, Pt, Pd, Ir) [34–38]. Therefore, creating defect sites and generating SMSI on the surface of a catalyst is an effective strategy to improve the oxidation capacity for HCHO.

In this study, through inducing surface defects of TiO_2 pretreated with different atmospheres (H_2/N_2, N_2, O_2/N_2) at the high temperature (800 °C), we tuned SMSI on Pd/TiO_2 catalysts. The effect of SMSI on the physical structures and chemical properties of Pd/TiO_2 catalysts was further investigated. As a case, the performance of HCHO oxidation on the catalysts with different SMSI was also studied.

The XRD patterns of the samples are shown in Fig. S1 (Supporting information). All of the XRD diffraction peaks were attributed to rutile TiO_2 [14] and there were no diffraction peaks observed of Pd species, which indicated that the Pd species were well-dispersed on all of the catalysts [39]. After treatment at high temperature, the specific surface areas of the samples were all notably decreased, from 33.0 m^2/g to 8.2, 12.5 and 13.8 m^2/g for the Pd/TiO_2–$800H_2$, Pd/TiO_2–$800N_2$ and Pd/TiO_2–800Air catalysts, respectively (Table 1). As we can see, the specific surface areas were similar for the Pd/TiO_2–$800N_2$ and Pd/TiO_2–800Air samples, but the area of Pd/TiO_2–$800H_2$ catalyst was smaller than them due to pore collapse induced by the strong reducing power of hydrogen.

As is well known, after high temperature treatment, the surface structure of materials undergoes changes. To investigate the structures of surface defects on the three kinds of carriers, ESR and UV–vis were carried out and the results are displayed in Fig. 1 and Fig. S2 (Supporting information). From the ESR results in Fig. 1a, the TiO_2–$800N_2$ and TiO_2–800Air samples exhibited similar ESR spectra with a single signal at $g = 2.003$, which was assigned to oxygen vacancies (V_o) [32,40]. By contrast, two signals were observed in the ESR spectrum of the TiO_2–$800H_2$ catalyst at $g = 2.003$ and $g = 1.962$, which were ascribed to V_o and Ti^{3+} defects, respectively [41–43]. The results indicated that abundant surface defects were formed on the TiO_2 carrier by the reducing atmosphere treatment at high temperature, which was in line with the UV–vis results (as shown in Fig. S2a).

After Pd loading, Similarly, as shown in the ESR results (Fig. 1b), only a weak V_o signal ($g = 2.004$) observed for all of the three catalysts. It is worth noting that a significantly larger Ti^{3+} signal ($g = 1.952$) was observed on the Pd/TiO_2–$800H_2$ sample. Meanwhile, the differences in defect density between the three catalysts were in accordance with the UV–vis measurement results (as shown in Fig. S2b). The results indicated that there were more defects formed on the Pd/TiO_2–$800H_2$ catalyst.

With low-surface-area supports, serious aggregation of loaded precious metals would occur [18]. Thus, the mean Pd particles size on the three Pd/TiO_2 catalysts calculated based on STEM images, and the result displayed in Table 1 and Fig. S3 (Supporting information). According to the results, the average particle size of Pd particles on the Pd/TiO_2–$800N_2$ and Pd/TiO_2–800Air catalysts were 3.3 and 3.4 nm, respectively. However, it was much smaller on the Pd/TiO_2–$800H_2$ catalyst, which was just 1.5 nm. Comparatively, the Pd particle size distribution was relatively uniform and most of them were in the monoatomic range (as shown in Table S1 in Supporting information). The phenomenon may be due to the presence of more surface defects, which was favored to anchor the precious metals, and further induced stronger MSI between Pd particles and the carrier [10,44].

In order to verify the existing of SMSI on the three catalysts, *in-situ* CO adsorption was carried out and the result was shown in Fig. S4 (Supporting information). There were two peaks in the spectra for the three catalysts. The peaks at low frequency (around 1980 cm^{-1}) were similar on the three catalysts and were assigned to bridge-bonded CO ($\upsilon(CO)_b$) on two Pd atoms [45], Another peak at higher frequency (around 2090.6 cm^{-1}) was ascribed to linear adsorption ($\upsilon(CO)_l$) of Pd-CO [7,46]. Notably, $\upsilon(CO)_l$ decreased gradually (in the order of Pd/TiO_2–800Air > Pd/TiO_2–$800N_2$ > Pd/TiO_2–$800H_2$), meanwhile the $\upsilon(CO)_b/\upsilon(CO)_l$ intensity ratio increased, which was attributed to the increase in the strength of the metal-support interaction (MSI) [47]. That is, the Pd/TiO_2–$800H_2$ catalyst possessed the strongest MSI.

According to previous work, TiO_{2-x} was prone to migrate to the noble metal surface because of the high surface energy at high temperature [16,48–50]. In view of Ti^{3+} species presence on the three catalysts, whether were the Pd particles enveloped by Ti^{3+} species? From the result of HRTEM (as shown in Fig. 2a), there were some amorphous thin film formed on the Pd particles on all of the catalysts, which indicated that SMSI was constructed, which was further verified by the result of EELS spectra. As shown in Figs. 2b-d. Line scans (along the green line in the picture) were performed in the vicinity of Pd particles. Clearly, there was no signal in the background region (region I), and a small signal of Ti species appeared in the amorphous overlayer on the Pd particle surface (region II); meanwhile, a large amount of Ti species was detected on the TiO_2 substrate (region III). It is worth pointing out that Ti species in the amorphous overlayer were only in the Ti^{3+} valence state (region II), which was different from the Ti species in the support, which existed in both Ti^{4+} and Ti^{3+} valence states (region III) (shown in Fig. S5 in Supporting information). Comparing the three catalysts, the amount of Ti^{3+} species in the amorphous overlayer of Pd particles increased gradually in the order Pd/TiO_2–$800H_2$ > Pd/TiO_2–$800N_2$ > Pd/TiO_2–800Air. This result clearly showed that Pd nanoparticles were encapsulated by TiO_{2-x} to varying degrees, and there was the strongest MSI formed on the Pd/TiO_2–$800H_2$ catalyst.

The evolution of Pd/TiO_2 catalysts subjected to pretreatment in different atmospheres was also investigated with X-ray absorption spectroscopy (XAS). Since the activity and structure of Pd/TiO_2–$800N_2$ and Pd/TiO_2–800Air are similar, here Pd/TiO_2–$800N_2$ was used as the representative sample for discussion. Fig. 3a displays the Fourier-transformed EXAFS spectra of the Pd K-edge for the Pd/TiO_2 catalysts. As seen in the figure, two main peaks were ob-

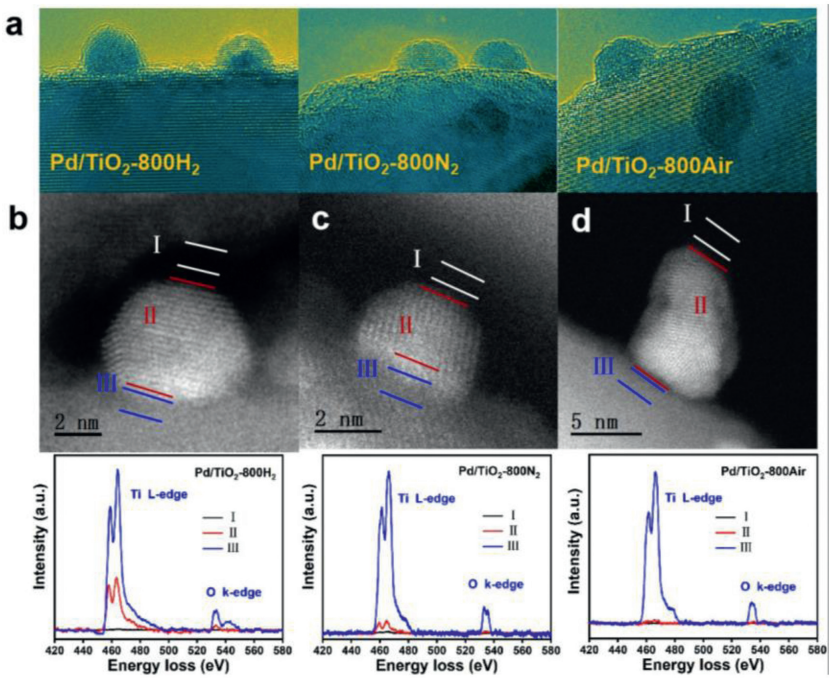

Fig. 2. (a) HRTEM, STEM and EELS spectra of (b) Pd/TiO_2–$800H_2$, (c) Pd/TiO_2–$800N_2$ and (d) Pd/TiO_2–800Air catalysts.

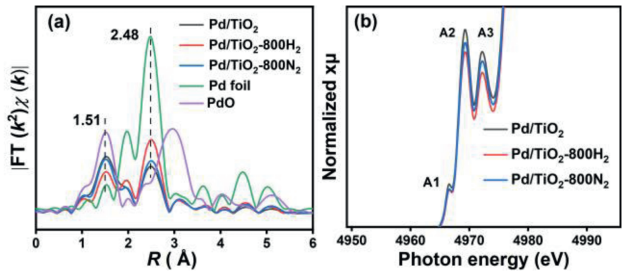

Fig. 3. (a) Fourier transforms of the k_2-weighted EXAFS of Pd K-edge for Pd foil, PdO, and the Pd/TiO_2-X catalysts (Pd/TiO_2, Pd/TiO_2–$800N_2$, Pd/TiO_2–$800H_2$ samples). (b) Ti K-edge XANES for the Pd/TiO_2-X catalysts (Pd/TiO_2, Pd/TiO_2–$800H_2$, Pd/TiO_2–$800N_2$ samples).

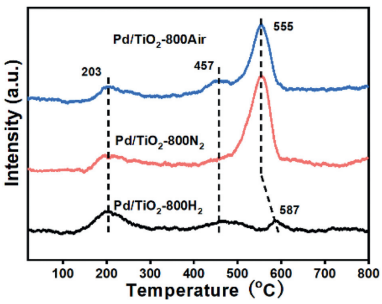

Fig. 4. O_2-TPD spectra of Pd/TiO_2–$800H_2$, Pd/TiO_2–$800N_2$ and Pd/TiO_2–800Air samples.

served. The peak at ~2.48 Å was associated with Pd-Pd pairs and another peak at 1.51 Å was assigned to Pd-O bonds [51]. Clearly, there were the most Pd-Pd pairs and fewest Pd-O bonds on the Pd/TiO_2–$800H_2$ catalyst. On the contrary, the most Pd-O pairs and fewest Pd-Pd bonds were found on the Pd/TiO_2 catalyst. The results indicated that Pd species in the metallic state were more stable on the Pd/TiO_2–$800H_2$ catalyst. On the other hand, the XANES spectra at the Ti K-edge for TiO_2 are displayed in Fig. 3b, and three peaks (A1, A2 and A3) were observed, which were associated with electron absorption in the 1 s orbital of Ti [52]. The three peaks exhibit a declining trend in peak intensities, in the order of Pd/TiO_2 > Pd/TiO_2–$800N_2$ > Pd/TiO_2–$800H_2$. The difference was due to the greater density of defects formed on the Pd/TiO_2–$800H_2$ catalyst, which was closely related to the TiO_{2-x} overlayer [49]. According to the test results, we speculate that the stability of Pd metals is closely related to the presence of TiO_{2-x} encapsulation layers.

As is well known, active oxygen was very important in oxidation reactions, which was closely related to precious metal site. Therefore, it is necessary to test the reactive oxygen ability of Pd/TiO_2 catalysts. From O_2-TPD results (displayed in Fig. 4), there were three peaks observed for all of the samples. The peak at 203 °C was ascribed to active oxygen species. The peak at 457 °C was assigned to the surface lattice oxygen of TiO_2. The last peak at 555 °C was ascribed to lattice oxygen of PdO [53], which was confirmed by the H_2-TPSR results (as shown in Fig. S6 in Supporting information). Clearly, there were more active oxygen species on the Pd/TiO_2–$800H_2$ catalyst than that on the Pd/TiO_2–$800N_2$ and Pd/TiO_2–800Air samples. It is worth noting that the Pd/TiO_2–$800N_2$ and Pd/TiO_2–800Air catalysts possessed more PdO species than the Pd/TiO_2–$800H_2$ catalyst, which may be attributed to the metallic Pd species being re-oxidized by O_2 to form PdO on the Pd/TiO_2–$800N_2$ and Pd/TiO_2–800Air catalysts. The results indicated that the metallic Pd species are more stable on Pd/TiO_2–$800H_2$ catalyst than that on the other two catalysts. Combined with the results of O_2-TPD and XAFS experiments, we could reasonably speculate that the stability of Pd species may be related to the interaction between metal and support.

In order to investigate catalyst stability, the CO adsorption experiment was carried out again. In this case, the samples were pretreated in air at 150 °C for 30 min (the aged catalysts were marked as Pd/TiO_2-$800H_2$-O_2, Pd/TiO_2-$800N_2$-O_2, Pd/TiO_2-800Air-O_2) and the spectra are displayed in Fig. S7 (Supporting information). Compared with the results of Figs. 2b-d and Fig. S4, after air pretreatment the CO *in situ* adsorption peaks presented an increasing trend; meanwhile, the $\upsilon(CO)_b/\upsilon(CO)_l$ ratio showed a decreas-

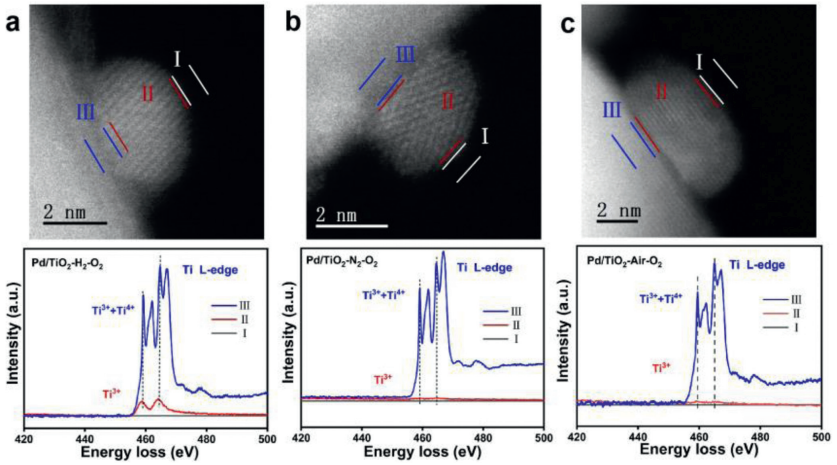

Fig. 5. STEM and EELS spectra of (a) Pd/TiO_2-800H_2-O_2, (b) Pd/TiO_2-800N_2-O_2 and (c) Pd/TiO_2-800Air-O_2 samples.

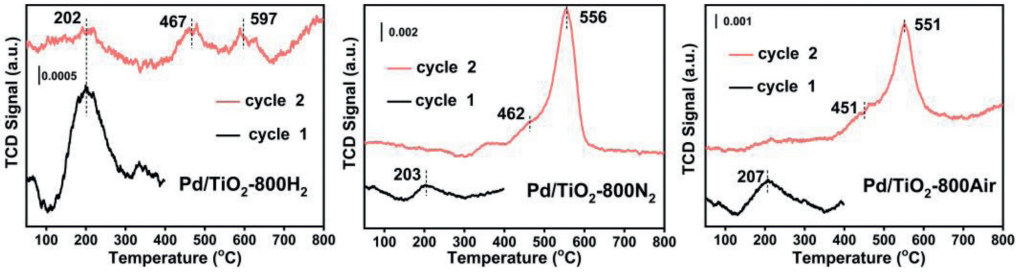

Fig. 6. O_2-TPD cycle test of Pd/TiO_2–800H_2, Pd/TiO_2–800N_2 and Pd/TiO_2–800Air samples, respectively.

ing trend, which suggested that the SMSI on the three catalysts decreased to different degrees. This may be due to the amorphous TiO_{2-x} coating on the noble metals being destroyed to different degrees.

To further investigate the change of SMSI, EELS spectra were collected on the three catalysts after mild oxygen treatment (shown in Figs. 5a-c). Compared with the spectra of Figs. 2b-d, the signals of Ti^{3+} species in the amorphous overlayer were reduced significantly, which suggested that the TiO_{2-x} coating had fallen off to different degrees on the three catalysts. However, there were still a large number of Ti^{3+} species on the Pd/TiO_2-800H_2-O_2 catalyst. The results further confirmed that the difference in catalyst stability is related to the amorphous TiO_{2-x} overlayer, which could protect the Pd particles, as the active sites, from being oxidized. However, there was no significant difference on the catalysts before and after oxidation treatment based on XPS results (shown in Fig. S8 and Table S2 in Supporting information). It may be due to the limited test accuracy of XPS, and it is difficult to accurately detect the changes of TiO_{2-x} species on the surface of Pd particles.

To further investigate the stabilities of Pd species, we carried out O_2-TPD cycle test (displayed in Fig. 6). Similar to Fig. 4, the cycle 1 test illustrated that active oxygen species were desorbed at 203 °C on all of the catalysts. It is worth mentioning that in the cycle 2 test, there were no active oxygen species observed on the Pd/TiO_2–800N_2 and Pd/TiO_2–800Air samples, in contrast to the Pd/TiO_2–800H_2 sample, where there were still some reactive oxygen species. The results showed that the Pd particles on Pd/TiO_2–800H_2 catalyst were more stable than on other two catalysts.

We take HCHO oxidation as a probe reaction. The HCHO oxidation performance at low temperature (10 °C) over Pd/TiO_2–800H_2, Pd/TiO_2–800N_2 and Pd/TiO_2–800Air catalysts are displayed in Fig. S9 (Supporting information). Pd/TiO_2–800H_2 catalyst displayed excellent HCHO oxidation reaction, and which could completely convert HCHO to CO_2 and H_2O at 10 °C. To investigate the effect of catalyst stability on the HCHO oxidation performance, we carried out the intrinsic activity test. Based on the results of Pd dispersion (D_{TEM}), turnover frequencies (TOF_s) over the three catalysts were calculated and the results are summarized in Table 1. Pd/TiO_2–800H_2, Pd/TiO_2–800N_2 and Pd/TiO_2–800Air catalysts presented TOFs of 2.68 × 10^{-2}, 1.69 × 10^{-2} and 1.12 × 10^{-2} s^{-1}, respectively, which was consistent with the apparent activity of the catalysts. Further, to explore the effect to catalyst activity, we tested the TOF of three catalysts, which were pretreated by air at 150 °C for 30 min. Compared to the fresh catalysts, the oxidation capacity of the samples with destroyed SMSI on the surface was greatly reduced (shown in Fig. 7). Among them, the Pd/TiO_2–800H_2 catalyst with strongest MSI displayed better activity and stability. Pd 3d XPS test results (shown in Fig. S10 and Table S2 in Supporting information) indicated that Pd species valence have

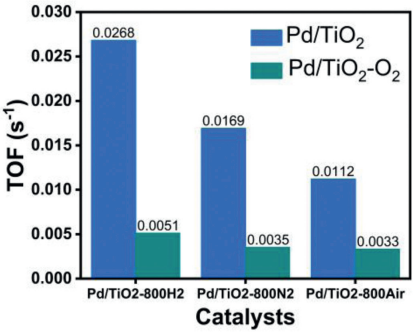

Fig. 7. The intrinsic activity of Pd/TiO_2 and Pd/TiO_2-O_2 catalysts. Reaction conditions: 10 °C, 150 ppm of HCHO, 20% O_2, 35% RH, He balance.

no obvious change for the three catalysts. There were two main reasons for this phenomenon: (1) HCHO oxidation reaction was carried out at relatively low temperature and most of Pd species maintained metallic state; (2) the changes of Pd species on the surface of Pd nano-particles were slightly and it is difficult to accurately detect by XPS. This article proves that SMSI improved stability of the active site of catalysts, which was important for expression of catalyst activity.

In summary, in order to study the influence of SMSI on the stabilities of catalysts, we tuned SMSI on Pd/TiO_2 catalysts through inducing surface defects of TiO_2 by pretreated with different atmospheres (H_2/N_2, N_2, O_2/N_2) at the high temperature (800 °C). Based on the results of characterization by various techniques, Ti^{3+} and V_o defects appeared on the surface of the carrier after high temperature treatment, and the defect content varied in the order Pd/TiO_2–$800H_2$ > Pd/TiO_2–$800N_2$ > Pd/TiO_2–800Air, which was in line with the reducing ability of the treatment gas. The Pd/TiO_2–$800H_2$ catalyst, with more surface defects, favored the construction of SMSI. It was proven by *in situ* CO adsorption and EELS tests that the Pd particles were encapsulated by TiO_{2-x} species, and the amorphous layer could efficiently stabilize the Pd particles remains in metallic state. In the probe reaction, the Pd/TiO_2–$800H_2$ catalyst, with stronger MSI, displayed better stability and HCHO oxidation performance than other two catalysts at low temperature (10 °C).

Declaration of competing interest

The authors declare that they have no known competing financial interests or personal relationships that could have appeared to influence the work reported in this paper.

Acknowledgments

This work was supported by the Youth Innovation Promotion Association, CAS (No. 2020310), the Science and Technology Planning Project of Xiamen City (No. 3502Z20191021), the Science and Technology Innovation “2025” major program in Ningbo (No. 2022Z028). This research used beamline 7-BM (QAS) of the National Synchrotron Light Source II, a U.S. Department of Energy (DOE) Office of Science User Facility operated for the DOE Office of Science by Brookhaven National Laboratory under Contract No. DE-SC0012704.

Supplementary materials

Supplementary material associated with this article can be found, in the online version, at doi:10.1016/j.cclet.2023.108739.

References

[1] S. Tauster, S. Fung, R. Garten, J. Am. Chem. Soc. 100 (1978) 170–175.
[2] T.W. van Deelen, C. Hernández Mejía, K.P. de Jong, Nat. Catal. 2 (2019) 955–970.
[3] R.M. Kennedy, L.A. Crosby, K. Ding, et al., Catal. Lett. 148 (2018) 2223–2232.
[4] J. Zhang, H. Wang, L. Wang, et al., J. Am. Chem. Soc. 141 (2019) 2975–2983.
[5] H. Li, X. Weng, Z. Tang, et al., ACS Catal. 8 (2018) 10156–10163.
[6] Q. Fu, H. Saltsburg, M. Flytzani-Stephanopoulos, Science 301 (2003) 935–938.
[7] J.C. Matsubu, S. Zhang, L. DeRita, et al., Nat. Chem. 9 (2016) 120–127.
[8] H. Tang, F. Liu, J. Wei, et al., Angew. Chem. Int. Ed. 55 (2016) 10606–10611.
[9] L. Nie, D. Mei, H. Xiong, et al., Science 358 (2017) 1419–1423.
[10] J. Wang, W. Chen, C. Jia, et al., Adv. Mater. 8 (2018) 1705369–1705377.
[11] K. Okumura, R. Yoshimoto, T. Uruga, et al., J. Phys. Chem. B 108 (2004) 6250–6255.
[12] S. Colussi, M. Boaro, L. de Rogatis, et al., Catal. Today 253 (2015) 163–171.
[13] D. Li, G. Yang, P. Li, J. Wang, P. Zhang, Catal. Today 277 (2016) 257–265.
[14] A. Naldoni, F. Riboni, M. Marelli, et al., Catal. Sci. Technol. 6 (2016) 3220–3229.
[15] Y. Li, C. Wang, C. Zhang, H. He, Top. Catal. 63 (2020) 810–816.
[16] H. Tang, Y. Su, B. Zhang, et al., Sci. Adv. 3 (2017) e1700231.
[17] Y. Zhang, J. Liu, K. Qian, et al., Angew. Chem. Int. Ed. 60 (2021) 12074–12081.
[18] N. An, W. Zhang, X. Yuan, et al., Chem. Eng. J. 215-216 (2013) 1–6.
[19] A.P. Jones, Atmos. Environ. 33 (1999) 4535–4564.
[20] F. Bianchi, M. Careri, M. Musci, A. Mangia, Food Chem. 100 (2007) 1049–1053.
[21] A. Aydogan, L.D. Montoya, Atmos. Environ. 45 (2011) 2675–2682.
[22] Y. Su, Y. Liang, J. Hazard. Mater. 291 (2015) 120–128.
[23] J.P. Bellat, I. Bezverkhyy, G. Weber, et al., J. Hazard. Mater. 300 (2015) 711–717.
[24] D. Kibanova, M. Sleiman, J. Cervini-Silva, H. Destaillats, J. Hazard. Mater. 211-212 (2012) 233–239.
[25] S. Sun, J. Ding, J. Bao, et al., Catal. Lett. 137 (2010) 239–246.
[26] C. Huang, Y. Ding, Y. Chen, et al., J. Environ. Sci. 60 (2017) 61–69.
[27] K. Li, J. Ji, Y. Gan, H. Huang, Chin. Chem. Lett. 33 (2022) 434–443.
[28] W. Liang, J. Li, J. Li, T. Zhu, Y. Jin, J. Hazard. Mater. 175 (2010) 1090–1095.
[29] B. Bai, Q. Qiao, H. Arandiyan, J. Li, J. Hao, Environ. Sci. Technol. 50 (2016) 2635–2640.
[30] G. Liu, J. Zhou, W. Zhao, Z. Ao, T. An, Chin. Chem. Lett. 31 (2020) 1966–1969.
[31] Y. Li, C. Zhang, J. Ma, et al., Appl. Catal. B 217 (2017) 560–569.
[32] C. Wang, Y. Li, C. Zhang, et al., Appl. Catal. B 282 (2021) 119540.
[33] X. Chen, G. He, Y. Li, et al., ACS Catal. 10 (2020) 9706–9715.
[34] Y. Li, X. Chen, C. Wang, C. Zhang, H. He, ACS Catal. 8 (2018) 11377–11385.
[35] C. Zhang, F. Liu, Y. Zhai, et al., Angew. Chem. Int. Ed. 51 (2012) 9628–9632.
[36] C. Zhang, Y. Li, Y. Wang, H. He, Environ. Sci. Technol. 48 (2014) 5816–5822.
[37] M. Huang, Y. Li, M. Li, et al., Environ. Sci. Technol. 53 (2019) 3610–3619.
[38] J. Chen, J. Ding, H. Li, et al., Catal. Sci. Technol. 9 (2019) 3287–3294.
[39] C. Yang, Z. Wang, T. Lin, et al., J. Am. Chem. Soc. 135 (2013) 17831–17838.
[40] S. Zhu, J. Zheng, S. Xin, L. Nie, Chem. Eng. J. 427 (2022) 130951.
[41] C. Kumar, N. Gopal, T. Wang, M. Wong, S. Ke, J. Phys. Chem. B 110 (2006) 5223–5229.
[42] J. Zheng, L. Liu, G. Ji, et al., ACS Appl. Mater. Inter. 8 (2016) 20074–20081.
[43] J. Li, M. Zhang, Z. Guan, et al., Appl. Catal. B 206 (2017) 300–307.
[44] J. Li, H. Zhou, H. Zhuo, et al., J Mater. Chem. A 6 (2018) 2264–2272.
[45] B. Qiao, A. Wang, X. Yang, et al., Nat. Chem. 3 (2011) 634–641.
[46] Y. Wang, D. Widmann, R. Behm, ACS Catal. 7 (2017) 2339–2345.
[47] C. Hippe, R. Lamber, G. Schulz-Ekloffand, U. Schuber, Catal. Lett. 43 (1997) 195–199.
[48] Y. Li, Y. Fan, H. Yang, et al., Chem. Phys. Lett. 372 (2003) 160–165.
[49] Y. Zhang, X. Yang, X. Yang, et al., Nat. Commun. 11 (2020) 3185–3192.
[50] S. Liu, W. Xu, Y. Niu, et al., Nat. Commun. 10 (2019) 5790–5798.
[51] T. Ishida, T. Honma, K. Nakada, et al., J Catal. 374 (2019) 320–327.
[52] L.X. Chen, T. Rajh, Z. Wang, M.C. Thurnauer, J. Phys. Chem. B 101 (1997) 10688–10697.
[53] J. Chen, Y. Wu, W. Hu, et al., Appl. Catal. B 264 (2020) 118475–118486.